

**Manuscript version: Author's Accepted Manuscript**

The version presented in WRAP is the author's accepted manuscript and may differ from the published version or Version of Record.

**Persistent WRAP URL:**

<http://wrap.warwick.ac.uk/116512>

**How to cite:**

Please refer to published version for the most recent bibliographic citation information. If a published version is known of, the repository item page linked to above, will contain details on accessing it.

**Copyright and reuse:**

The Warwick Research Archive Portal (WRAP) makes this work by researchers of the University of Warwick available open access under the following conditions.

Copyright © and all moral rights to the version of the paper presented here belong to the individual author(s) and/or other copyright owners. To the extent reasonable and practicable the material made available in WRAP has been checked for eligibility before being made available.

Copies of full items can be used for personal research or study, educational, or not-for-profit purposes without prior permission or charge. Provided that the authors, title and full bibliographic details are credited, a hyperlink and/or URL is given for the original metadata page and the content is not changed in any way.

**Publisher's statement:**

Please refer to the repository item page, publisher's statement section, for further information.

For more information, please contact the WRAP Team at: [wrap@warwick.ac.uk](mailto:wrap@warwick.ac.uk).

# Temperature Considerations for Charging Li-ion Batteries: Inductive vs. Mains Charging Modes for Portable Electronic Devices

Over the last decade, the world has witnessed the competitive development of so-called “smart-phone” technologies, with increasing levels of functionality. Contemporary pocket-sized devices now have PC-like capabilities. Such a collection of processing capability creates a very demanding duty cycle for the battery, which is required to supply power to several components simultaneously. This includes the CPU, memory, touchscreen, graphics hardware, audio functions, storage and many networking interfaces.<sup>1</sup> The functionality of such devices has increased at a fast pace. As such there is an increasing drive to manufacture higher capacity Li-ion batteries (LIBs) with faster charging capabilities, in order to meet the requirements of processing power. A key constraint to progress in identifying newer chemistries, with increasing battery capacity, is the requirement to retain stability in diverse operating environments. Battery formats used within smart-phones have a limited volume, for practical reasons of packaging them into the device, thus a limited achievable power. This reflects how much energy they can store and how quickly they can deliver this.

Inductive charging technology is attracting a wide range of applications, from low-power applications (such as mobile phones) to charging for electric vehicles, owing to its convenience and better user experience.<sup>2</sup> Despite having been pioneered over 100 years ago by Nikola Tesla, inductive charging has only relatively recently been considered as a potential game-changer with today’s applications. In 2017, fifteen automobile models have announced the inclusion of consoles within vehicles for inductively charging consumer electronic devices, such as smartphones.<sup>3</sup>

Near-field magnetic coupling is the inductive mode used for battery charging in the consumer electronics industry. Inductive charging enables a power source to transmit energy to an electrical load across an air gap, without the use of connecting wires<sup>2</sup>. Such systems use AC mains to DC, then DC to high frequency AC conversion with an air-core transformer operating in the radio frequency (RF) domain to accomplish near-field magnetic coupling.

One of the main issues with this mode of charging is that of thermal management. There are several

sources of heat generation associated with any inductive charging system, as depicted in Figure 1.

Eddy currents are circulating electrical currents induced in a conductive material by a changing magnetic field, resulting in localised Joule heating. Since the device and charging base are in close physical contact, heat generated is transferred to the device by simple thermal conduction and convection.

The receiving antenna (device side) is close to the back cover of the phone, which is usually electrically non-conductive – see Figure S1 in Supplementary Information (SI) for a simplified device and charger schematic illustration.<sup>4</sup> Packaging constraints necessitate placement of the battery in close proximity to the receiving antenna and power electronics, with limited opportunities to dissipate or shield it from heat generated by the above mechanisms.<sup>5</sup> The ambient temperature and airflow in the environment surrounding a charging phone will have an influence on the temperature maxima experienced by the phone battery.

Magnetic fields in electrochemical systems have also been observed to influence mass transport, electrode kinetics and electrochemical equilibria via 3 mechanisms:<sup>6</sup>

- (i) Exertion of Lorentz forces on charged species – see Figure S2 in SI
- (ii) Force generation where there is a gradient in magnetic energy.
- (iii) Weak perturbations of chemical potential for systems within very high magnetic fields.

The position of the phone on the inductive charging base was investigated to establish whether this could affect the resulting temperature of the phone during charging. More specifically the deliberate misalignment of transmitter and receiver coils (in x and z directions) was performed with simultaneous charging and thermal imaging to capture time-resolved heat generation. This generates temperature maps to help quantify the heating effects.

Issue around alignment have been observed during the process of inductive charging by way of the measured efficiency as a function of alignment. To compensate for poor alignment, inductive charging systems typically increase

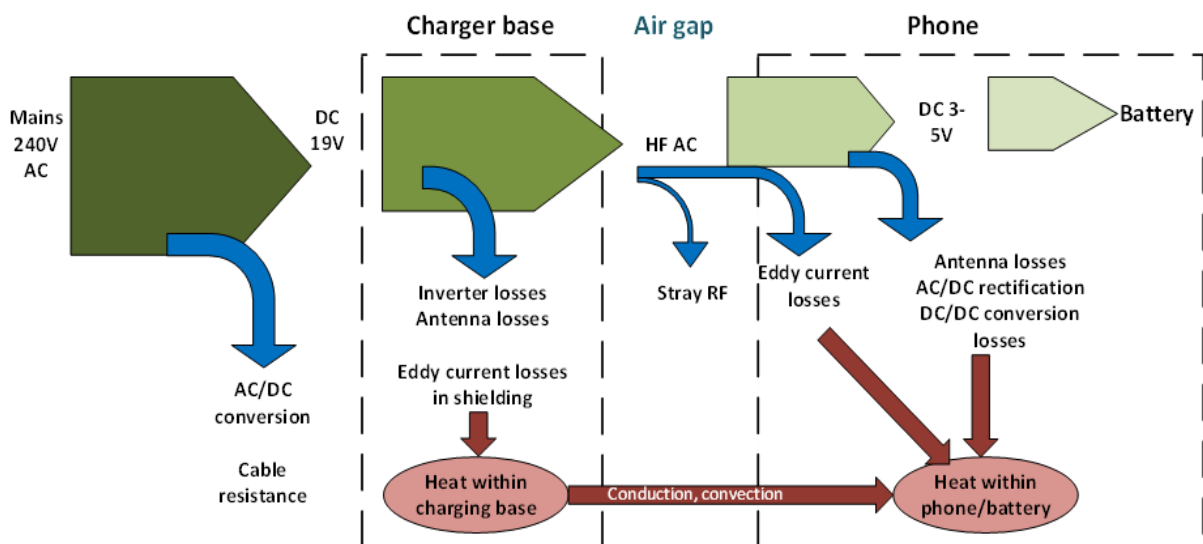


**Figure 1. Schematic illustration of the sources of energy loss (inefficiency) and heat generation during inductive charging.**

the transmitter power and/or adjust its operating frequency, which incurs further efficiency losses and increases heat generation.<sup>7</sup>

The other drawback is the short range required to optimise this efficiency, which means that the receiving device must be very close to the transmitter (induction unit) in order to inductively couple with it. Newer approaches can diminish these transfer losses by using ultra-thin coils, higher frequencies and optimized drive electronics to provide chargers and receivers that are compact, more efficient and can be integrated into mobile devices or batteries with minimal change.<sup>8</sup> In 2017, there were several reports in the press about battery problems with some of the newly released iPhone 8 Plus phones. A few reports showed that the phones were physically splitting apart soon after they began to be used.<sup>9</sup>

It has been well documented that increased calendar aging occurs in batteries as a function of storage temperature.<sup>10</sup> Temperature can thus significantly influence the state-of-health (SoH) of batteries over their useful lifetime and is schematically represented in Fig. 2.<sup>11</sup> The Arrhenius equation (Equation 1) accurately demonstrates the temperature dependence of reaction rate constants and provides useful characterisation tool of the rates of battery (electro)chemical reactions. It is also valid for side reactions (parasitic reactions) leading to battery degradation such as decomposition of active materials or build-up of passivating films. This means that the higher the temperature the faster the battery ages.

$$k = Ae^{-\frac{E_a}{RT}} \quad (1)$$

Where  $k$  = Rate constant,  $Ae$  = Pre-exponential factor,  $E_a$  = Activation energy ( $\text{J mol}^{-1}$ ),  $R$  = Gas constant  $- 8.314 \text{ J mol}^{-1} \text{ K}^{-1}$  and  $T$  = Temperature (K). The rule of thumb with the Arrhenius equation is that for most chemical reactions, the reaction rate doubles with each  $10^\circ\text{C}$  rise in temperature - though this is an oversimplification.<sup>12</sup> One of the effects of ambient temperature increase on battery life can be reflected in the accelerated growth rate of passivating films on the cell's electrodes. This occurs by way of cell redox reactions, which irreversibly increase the internal resistance of the cell, ultimately resulting in performance failure. Leng *et al*, investigated battery performance within the temperature range  $25\text{-}55^\circ\text{C}$  and observed the predominance of electrode degradation, but also characterised rates of degradation in other cell components.<sup>13</sup> A battery dwelling above  $30^\circ\text{C}$  is considered to be at elevated temperature and exposing the battery to high temperature and dwelling in a full state-of-charge (SoC) for an extended time can be more stressful than cycling.<sup>14</sup> Arrhenius relationships

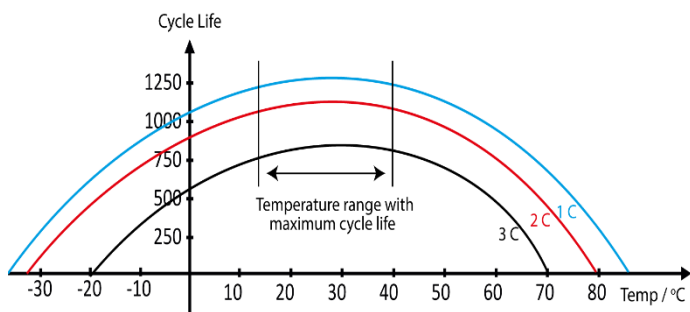


**Figure 2. The Effect of Ambient Temperature on LIB Cycle Life.**

provide some understanding of the influence of side reactions (parasitic) on battery degradation.

A similar consideration can be given to the SoC level, and as this gets closer to the saturation point the higher the rate of side reactions become. Degradation processes slow down over time such that aging effects typically depend on the square root of time. To account for these effects, an extended Arrhenius equation can be proposed and is useful for simulation purposes – see Equation 2.<sup>15</sup>

$$T_{Age} = A_0 e^{\frac{SoC - SoC_0}{b} \times \frac{T - T_0}{c} \times \sqrt{t}} \quad (2)$$

Where  $T_{Age}$  = Calendar aging,  $SoC_0$  and  $T$  and  $T_0$  are absolute temperatures,  $b$  and  $c$  = model parameters for SoC and  $T$  respectively and  $t$  = ageing time (days).

This describes the aging rate proportional to  $\sqrt{t}$  and the factor  $A_0$  scales the trend of the  $\sqrt{t}$ -function to the actual aging behaviour of the respective battery cell at reference conditions  $SoC_0$  and  $T_0$ . During lithiation-delithiation processes the solid-state diffusion of  $Li^+$  limits the rate at which charge and discharge can efficiently occur. This diffusion is also influenced by temperature, obeying Eyring's expression as outlined in Equation 3.

$$D_s = D_s^0 - \left( \frac{E_a}{RT} \right) \quad (3)$$

Guidelines issued by LIB manufacturers specify that the upper operational temperature range of their products should not surpass the 50-60 °C range to avoid gas generation and premature aging.<sup>16</sup> Basic investigations into the aging processes in batteries are complicated because batteries are multifaceted systems. The aging dynamics can be challenging to characterise also because time-dependent capacity- and power-fade do not originate from one single cause. Aging mechanisms typical for anodes and cathodes can differ significantly<sup>17</sup> but will not be comprehensively addressed for the purposes of this viewpoint.

Our investigation focuses on characterising operational ambient temperatures and how they can be influenced by charging modes. We compare the effects of mains AC versus Qi inductive charging (and phone positioning on the inductive charging base) and consider how these temperature changes could impact battery life, exploring probable root causes of performance degradation.

As a benchmark temperature study, Panasonic 3 Ah cells were subjected to long-term cycling at room and elevated temperatures. Figure S3 (a) in the SI shows a plot of normalised capacity percentage as a function of time for these 18650 cylindrical cells (based on graphite/NCA chemistry). It can be seen that the cells over

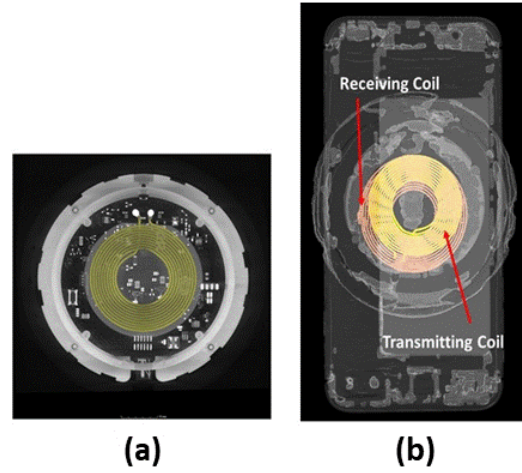


**Figure 3.** X-ray tomography scans of (a) Mophie charging base, and (b) the phone on top of the wireless charging base placed centrally.

the 18-month duration in a 45 °C environment show more pronounced aging effects in terms of capacity loss than the same test carried out on cells at 25 °C. In parallel, the plot in Figure S3 (b) shows the increase in internal resistance at this raised temperature.

The SoH of a battery, as a result, reduces over time because of these irreversible physical and chemical processes that constitute and drive degradation.<sup>18</sup> Such effects become increasingly critical when a large number of cells are connected in parallel, as is the case with high capacity battery systems required for Electric Vehicle (EV) applications.

Another source of material degradation in batteries is corrosion. Corrosion phenomena have been investigated in a study on aluminium current collectors at temperatures of 25 and 45°C where it was established that there is an increase in pit area in electrolytes based on  $LiPF_6$ .<sup>19</sup> (this is illustrated in Figure S4) Conversely, the copper foil in the negative electrode has been reported to be susceptible to corrosion by residual water in the organic solvents of the electrolyte.<sup>20</sup> Specifically pitting corrosion has been reported as the mechanism with corrosion products being composed of copper fluorides and copper oxides<sup>19</sup> from the existence of ionic F or P within the solvents.

Generally, ambient temperature increases are well known to be accelerating factors in corrosion processes<sup>21-22</sup> and can influence kinetic parameters of reactions.<sup>21</sup> This relates to corrosion mechanisms involving chemical reactions whose rates are temperature dependent - as described earlier in the Arrhenius Equation (1).

X-ray CT scan reveals on Mophie charging base, Figure 3 (a), shows that the transmitting coil comprised of 10 wire turns with 43.5 mm diameter

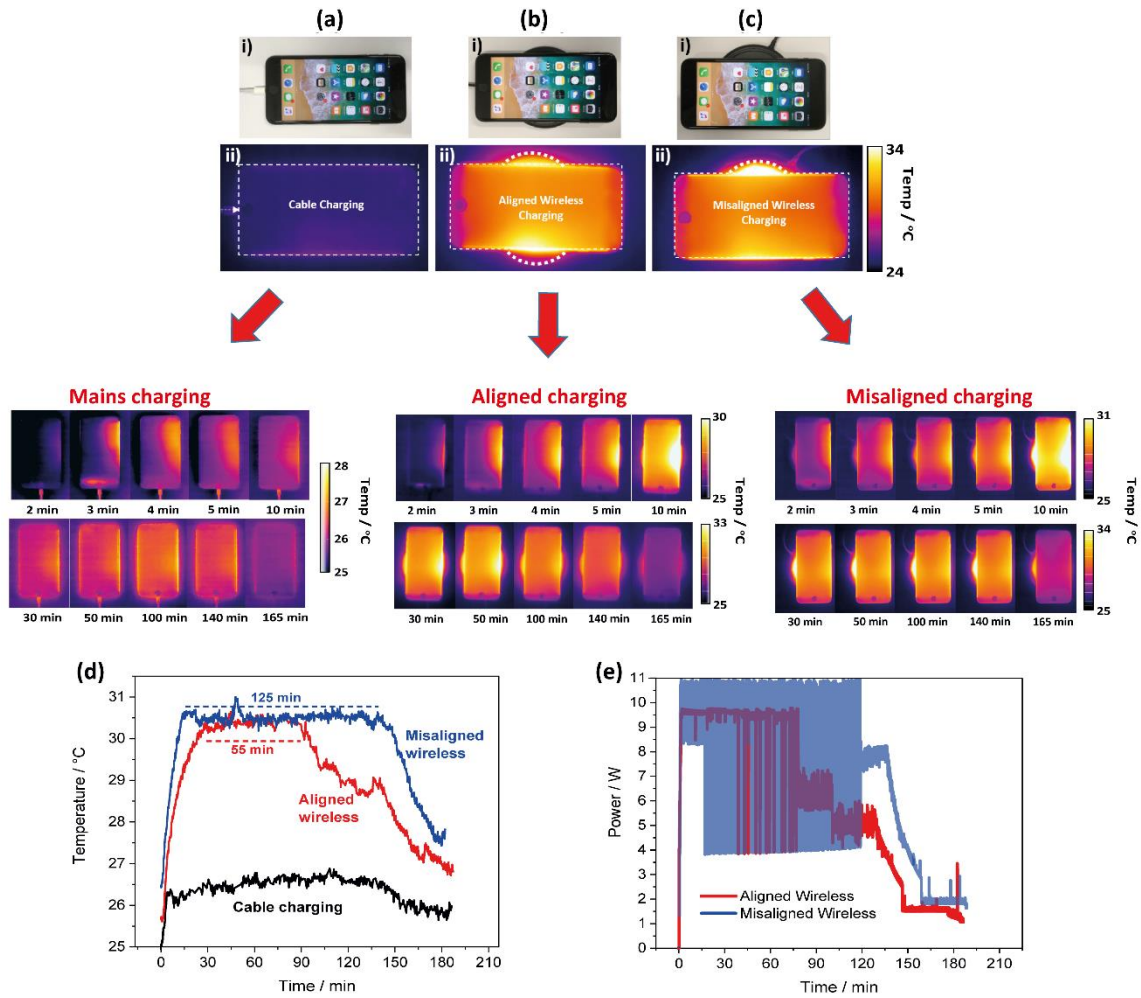


**Figure 4. Thermal imaging of the three modes of iPhone 8 Plus charging: (a) (i) Mains-driven cable charging, (b) (i) wireless charging where the phone coil is aligned with the coils of the charging base and (c) (i) where the coils are misaligned. (a-c) (ii) show the thermal profiles of the phone after 50 minutes of charging. (d) Graph show the temperature variation with time for the different modes of charging and (e) shows the power input during charging.**

located at the centre of the base. Additional CT scan was also performed on the phone placed centrally on the top of the charging base, assuming the receiving coil of the phone is aligned with the transmitting coil of the charging base, Figure 3 (b). CT scan, however shows that the coils are not perfectly aligned. This highlights that misalignment of the coils is a phenomenon that is difficult to avoid for a typical consumer. This can result in the charging base consuming more power as the frequency needs to readjust to optimise the coupling in order to maximise the power transfer efficiency.

Figure 4 illustrates three modes of charging, based on: (a) ac mains charging (cable charging), (b) inductive charging when coils are aligned and (c) misaligned. Figure 4 (a-c) (i) and (ii) show a realistic view of the charging modes with a snapshot of the thermal maps of the phone after 50 minutes of charging. Regardless of the mode of charging, the right edge of the

phone showed higher rate of increase in temperature than other areas of the phone and remained higher throughout the charging process. A CT scan of the phone, Figure S5 (a), shows this hotspot is where the motherboard is located. An average temperature plot versus time for the different charging modes are shown in Figure 4 (d). For these three modes, the phone required on average 180 minutes to be fully charged from 0 % SoC

With conventional mains power, the maximum average temperature reached within three hours of charging does not exceed 27 °C. In contrast to aligned inductive charging, the temperature peaked to 30.5 °C but gradually reduced for the latter half of the charging period. This is similar to the maximum average temperature observed during misaligned inductive charging. In the case of misaligned inductive charging, the peak temperature was of similar magnitude (30.5°C) but was reached sooner and persisted much

longer at this level (125 vs 55 minutes). Power input during aligned and misaligned inductive charging, Figure 4 (e), shows different power profiles. For aligned inductive charging, the power input reached 9.5 W and was stable at this level for ~40 minutes before fluctuating between 4 - 9.5 W. This coincides with the period when the phone average temperature plateaued at 30.5 °C for 55 minutes, Figure 4 (d). The power input then decreased in stages, resulting in temperature drop and this continued until the phone reached 100 % SoC.

In contrast, for misaligned inductive charging, the power input oscillated between 8.3 and 11.0 W from 0 % SoC for 15 minutes, followed by an increase in oscillation amplitude achieving between 4 - 11.0 W for 105 minutes. This coincides with the period when the average phone temperature was stable at 30.5 °C for 125 minutes. Variation of the power input observed in the two different charging scenarios indicates that the battery management system (BMS) and/or inductive charging system was regulating the rate of charging to avoid overheating. The temperature threshold for de-rating the charging power appeared to be around 32 °C, with the power input to the charging base oscillating between full power and the de-rate power (4W) in accordance with the internal phone/battery temperature.

Also noteworthy is the fact that the maximum input power to the charging base was greater for the misaligned case (11W) than the well-aligned case (9.5W). This is due to the charging system increasing the transmitter power under misalignment in order to maintain target input power to the device.

The maximum average temperature of the charging base whilst charging under misalignment reached 35.3 °C, two degrees higher than the temperature detected when the phone was aligned, which achieved 33 °C. This is symptomatic of deterioration in system efficiency, with additional heat generation attributable to power electronics losses and eddy currents. Inductive charging efficiency was further investigated by varying the z distance of the phone from charging base, as shown in Figure S6 and S7. Moreover, the effect of temperature on the charging current was studied, with results presented in Figure S8.

In addition to the thermal studies, we have briefly conducted electromagnetic field measurements comparing phone positions on the charging base i.e. aligned vs misaligned scenario. A magnetic probe was swept over the XY plane just above the surface of the phone whilst positioned flat on the charging base, as illustrated in Figure S9. The phone was positioned by hand to visually perfect alignment and to the most extreme misalignment position (in Y) that would still have the charger operating. The voltage induced in the probe is proportional to the magnitude of the magnetic field, and the cycle RMS voltage was recorded. As

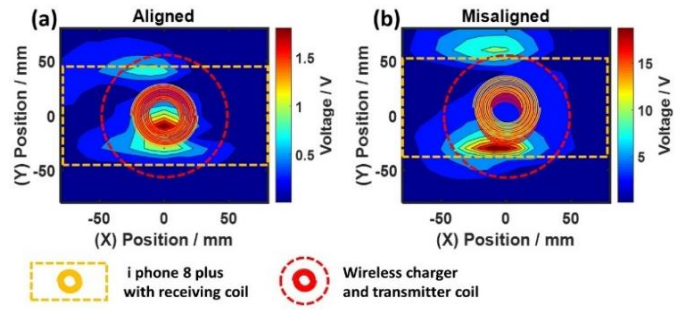


**Figure 5. Measuring the lost magnetic field during inductive charging. (a) Where the phone coil is aligned with the coils of the charging base and (b) where the two coils are misaligned.**

can be seen in Figure 5, the voltages obtained for when the phone is aligned to the charging base are an order of magnitude smaller than when the phone is misaligned. Through misalignment we reduce the efficiency of the magnetic inductive coupling between the coils in the phone and charger base which can result in a greater loss of magnetic field (leakage inductance), shown in Figure 5 (b). To compensate for the loss, the charging base appears to generate a greater magnitude of field resulting in these higher measured voltages. In addition, this compensates for the difference in flux that the phone coil experiences, and therefore the power into the phone can be maintained.

The energy efficiency of inductive charging therefore depends strongly on the coupling between the receiver and transmitter coils. Further work is needed to establish to what extent the increase in power demand by the charging base is caused by increasing input power, or by losses due to frequency tuning away from the optimal operating point of the charging base inverter.

Here we have demonstrated that more heat generation is induced from inductive charging of the iPhone 8 plus, than with conventional AC mains charging. Additional localised heat was generated from y- and z-plane misalignment of the phone with respect to the charging base. A greater magnitude of magnetic field was generated to compensate the leakage inductance due to loose coupling between transmitting and receiving coil resulting from misalignment. Consequently, this results in inefficient energy transfer during inductive charging, with electrical energy being converted to heat by way of eddy currents.

The increase in phone temperature during inductive charging at controlled temperatures is constrained by the BMS and charging system. Our findings show that when the phone charged via induction at 20 °C, the charging time reduced without overheating the phone. Under uncontrolled environment (26 °C starting temperature), the phone temperature continued to rise

and remained heated throughout the charging process. Hence, this highlights the importance of the BMS to regulate the power input during charging to prolong the phone's battery performance.

In addition to temperature-accelerated side reactions on the electrodes leading to progressive increases in internal resistance, many studies have investigated the effects of corrosion on current collectors and how such phenomena can impact the build-up of resistance within LIBs over their operational lifetime.<sup>19</sup> Several studies focused on the corrosion behaviour of aluminium current collectors, reporting localized corrosion being attributable to the electrolyte salt LiPF<sub>6</sub>.<sup>23</sup> On the negative electrode the copper current collector is also subjected to continuous corrosion in the organic conductive solution because of the residual water content of the organic solvents. With inductive charging becoming more common, and if heat generation from inductive charging is not a significant consideration in designing phone devices, the amount of swelling can be more significant.

Systems for conversion and transformation of energy are often subject to unwanted generation of heat. As mobile phones continue to get thinner, larger and smarter, their battery capacity will need to increase in parallel, to meet the power density requirements. To maximize a battery's effective lifetime, the temperature of its operating environment needs to be considered. Small increases in ambient temperature have been shown, in this study, to accelerate the rate of degradation, and decrease the battery's storage capacity, in commercial cylindrical cells. As inductive charging capabilities continue to develop for larger battery formats, there will also be a need to mitigate unwanted heat generation during charging times. We have highlighted how positioning the phone on the inductive charging base impacts the external temperature of the phone and relating charging currents, indicating desired conditions for a longer battery performance. Also shown was the effect of phone accessories such as the protective casing, which is dependent on the material type and thickness. In short, the evolution of higher power density devices capable of inductive charging will require manufacturing innovations in antenna materials and fabrication technologies, better magnetic shielding and heat dissipation.

\*Melanie. J. Loveridge, Chaou C. Tan, Faduma. M. Maddar, Guillaume Remy, Mike Abbott, Shaun Dixon, Richard McMahon, Ollie Curnick, Mark Ellis, Mike Lain, Anup Barai, Mark Amor-Segan, Rohit Bhagat and Dave Greenwood

Warwick Manufacturing Group (WMG), University of Warwick, Gibbet Hill Road, Coventry, CV4 7AL

## ASSOCIATED CONTENT

### Supporting Information.

The Supporting Information is available free of charge on the ACS Publications website at DOI:

Experimental section and additional results on z-plane wireless charging misalignment and temperature effect on charging current.

## AUTHOR INFORMATION

### Corresponding Author

\*E-mail: [M.Loveridge@warwick.ac.uk](mailto:M.Loveridge@warwick.ac.uk)

### Notes

Views expressed in this Viewpoint are those of the authors and not necessarily the views of the ACS. The authors declare no competing financial interest.

## ACKNOWLEDGMENT

This work was supported by HVM Catapult and The Faraday Institution Degradation Project (EP/S003053/1).

## REFERENCES

- (1) Carroll, A.; Heiser, G., An analysis of power consumption in a smartphone. In *Proceedings of the 2010 USENIX conference on USENIX annual technical conference*, USENIX Association: Boston, MA, 2010; pp 21-21.
- (2) Lu, X.; Wang, P.; Niyato, D.; Kim, D. I.; Han, Z., Wireless Charging Technologies: Fundamentals, Standards, and Network Applications. *IEEE Communications Surveys & Tutorials* **2016**, *18* (2), 1413-1452.
- (3) Smith, N. Tuning Qi and AirFuel/PMA Inductive Resonance Circuits for Optimal Efficiency. <https://www.idt.com/document/whp/tuning-qi-and-airfuel-pma-inductive-resonance-circuits-optimal-efficiency> (accessed 26 November 2018).
- (4) Johns, B.; Siddabattula, K.; Sengupta, U., Adapting Qi-compliant wireless-power solutions to low-power wearable products. *Analog Applications Journal* **2014**, *2Q*, 7.
- (5) Kerin, A. The Thermal Efficiency Behind Smartphone Trends. <https://www.qualcomm.com/news/onq/2013/10/09/thermal-efficiency-snapdragon-processors-under-screen-and-behind-trends> (accessed 3 December 2018).
- (6) Coey, M.; Hinds, G., *Magneto-electrolysis - the effect of magnetic fields in electrochemistry*. 2002.
- (7) A brief history of the Qi specification. <https://www.wirelesspowerconsortium.com/developers/specification.html> (accessed 17 December 2018).
- (8) Genieser, R.; Ferrari, S.; Loveridge, M.; Beattie, S. D.; Beanland, R.; Amari, H.; West, G.; Bhagat, R., Lithium ion batteries (NMC/graphite) cycling at 80 °C: Different electrolytes and related degradation mechanism. *Journal of Power Sources* **2018**, *373*, 172-183.
- (9) Apple investigating swollen batteries in iPhone 8 Plus handsets. <https://www.bbc.co.uk/news/technology-41551596> (accessed 3 December 2018).
- (10) Keil, P.; Schuster, S. F.; Wilhelm, J.; Travi, J.; Hauser, A.; Karl, R. C.; Jossen, A., Calendar Aging of Lithium-Ion Batteries: I. Impact of the Graphite Anode on Capacity Fade. *Journal of The Electrochemical Society* **2016**, *163* (9), A1872-A1880.

- (11) Rezvanizani, S. M.; Liu, Z.; Chen, Y.; Lee, J., Review and recent advances in battery health monitoring and prognostics technologies for electric vehicle (EV) safety and mobility. *Journal of Power Sources* **2014**, *256*, 110-124.
- (12) Vetter, J.; Novák, P.; Wagner, M. R.; Veit, C.; Möller, K. C.; Besenhard, J. O.; Winter, M.; Wohlfahrt-Mehrens, M.; Vogler, C.; Hammouche, A., Ageing mechanisms in lithium-ion batteries. *Journal of Power Sources* **2005**, *147* (1), 269-281.
- (13) Leng, F.; Tan, C. M.; Pecht, M., Effect of Temperature on the Aging rate of Li Ion Battery Operating above Room Temperature. *Scientific Reports* **2015**, *5*, 12967.
- (14) Bandhauer, T. M.; Garimella, S.; Fuller, T. F., A Critical Review of Thermal Issues in Lithium-Ion Batteries. *Journal of The Electrochemical Society* **2011**, *158* (3), R1-R25.
- (15) Dvorak, D.; Popp, H.; Bäuml, T.; Simic, D.; Kapeller, H., Arrhenius-Equation Based Approach for Modelling Lithium-Ion Battery Aging Effects. In *ITI Symposium*, Dresden, Germany, 2014.
- (16) Leenson, I. A., Old Rule of Thumb and the Arrhenius Equation. *Journal of Chemical Education* **1999**, *76* (10), 1459.
- (17) Christen, R.; Rizzo, G.; Gadola, A.; Stöck, M., Test Method for Thermal Characterization of Li-Ion Cells and Verification of Cooling Concepts. *Batteries* **2017**, *3* (1), 3.
- (18) Xiao, L.; Niyato, D.; Ping, W.; Dong In, K.; Zhu, H., Wireless charger networking for mobile devices: fundamentals, standards, and applications. *IEEE Wireless Communications* **2015**, *22* (2), 126-135.
- (19) Shuowei Dai, J. C., Yanjie Ren, Zhimin Liu, Jianlin Chen, Cong Li, Xinyuan Zhang, Xiao Zhang and Taofang Zeng, Electrochemical Corrosion Behavior of the Copper Current Collector in the Electrolyte of Lithium-ion Batteries. *International Journal of Electrochemical Science* **2017**, *12* (11), 10.
- (20) Zhao, M.; Kariuki, S.; Dewald, H. D.; Lemke, F. R.; Staniewicz, R. J.; Plichta, E. J.; Marsh, R. A., Electrochemical Stability of Copper in Lithium-Ion Battery Electrolytes. *Journal of The Electrochemical Society* **2000**, *147* (8), 2874-2879.
- (21) Pour-Ghaz, M.; Isgor, O. B.; Ghods, P., The effect of temperature on the corrosion of steel in concrete. Part 1: Simulated polarization resistance tests and model development. *Corrosion Science* 2009, *51* (2), 415-425.
- (22) Pour-Ghaz, M.; Burkan Isgor, O.; Ghods, P., The effect of temperature on the corrosion of steel in concrete. Part 2: Model verification and parametric study. *Corrosion Science* 2009, *51* (2), 426-433.
- (23) Zhang, X.; Winget, B.; Doeff, M.; Evans, J. W.; Devine, T. M., Corrosion of Aluminum Current Collectors in Lithium-Ion Batteries with Electrolytes Containing LiPF<sub>6</sub>. *Journal of The Electrochemical Society* 2005, *152* (11), B448-B454.